Interplay between London Dispersion, Hubbard U, and Metastable States for Uranium Compounds

Matthew S. Christian,*,† Erin R. Johnson,*,‡ and Theodore M. Besmann¶

Nuclear Engineering Program, University of South Carolina, Columbia, SC, Department of Chemistry, Dalhousie University, 6274 Coburg Road, Halifax, Nova Scotia, Canada B3H 4R2, and Center for Heirarchial Waste Form Materials (CHWM), University of South Carolina, Columbia, SC

E-mail: mchristi@cec.sc.edu; erin.johnson@dal.ca

Abstract

High-throughput computational studies of lanthanide and actinide chemistry with density-functional theory are complicated by the need for Hubbard U corrections, which ensure localization of the f electrons, but can lead to metastable states. This work presents a systematic investigation of the effects of both Hubbard U value and metastable states on the predicted structural and thermodynamic properties of four uranium compounds central to the field of nuclear fuels: UC, UN, UO_2, and UCl_3. We also assess the impact of the exchange-hole dipole moment (XDM) dispersion correction on the computed properties. Overall, the choice of Hubbard U value and inclusion of a dispersion correction cause larger variations in the computed geometric properties than result from metastable states. The weak dependence of structure optimization on metastable states should simplify future high-throughput calculations on actinides. Conversely, addition of the dispersion correction is found to offset the repulsion introduced by the Hubbard U term and provides greatly improved agreement with experiment for both cell volumes and heats of formation. The XDM dispersion correction is largely invariant to the chosen U value, making it a robust dispersion correction for actinide systems.

1 Introduction

Efforts continue for development of more efficient and robust nuclear fuels and to improve actinide waste-form materials for safe disposal of legacy nuclear wastes.[1–3] High-throughput computational screening is a powerful tool to complement experiment in the search for these new materials with targeted properties.[4–7] However, there is understandable hesitancy in applying high-throughput methods to materials containing f-block elements, as they can require additional corrections outside of traditional computational approaches used for main-group elements.[8–11]

Introduction of metastable electronic states is one particular barrier to obtaining accurate formation enthalpies for f-block materials with density-functional theory (DFT).[11–17] Most functionals typically used for solid-state applications incorrectly predict many semiconductors to have metallic states.[18–20] This is caused by delocalization error,[21–23] which arises from the semi-local nature of the exchange-correlation functionals that, for generalized gra-

*To whom correspondence should be addressed
†University of South Carolina
‡Dalhousie University
¶University of South Carolina

dient approximations (GGAs), depend only on the local electron density and its derivatives. Adding a Hubbard U correction[24–26] helps localize f-orbital electrons to a single atom by adding an energy barrier between orbital states.[9,27,28] However, this can result in convergence to a metastable state, higher in energy than the ground state, due to a suboptimal set of orbital occupations.[9,29,30] Convergence to such metastable states can result in calculated formation enthalpies that are far from experiment. Metastable states may also affect optimization of structures, as the forces used for structural relaxation are calculated from derivatives of the total energy. If the computed energies are unphysical, it is possible that the optimized structure will deviate significantly from experimental reality.[16]

There are currently three popular approaches used to avoid metastable states in GGA+U calculations: simulated annealing,[31] U-ramping,[30] and occupational matrix control (OMC).[12] Simulated annealing adds a randomly fluctuating external potential, which is gradually suppressed, to map the electronic potential energy surface in search of the ground state.[31] U-ramping is a procedure where the U potential is gradually increased from zero to a target value in small intervals.[30] OMC calculates energies for all possible f-orbital occupations, although this requires knowledge of the oxidation state for the actinide or lanthanide element.[12] Previous studies have been carried out to compare the ability of U-ramping and OMC to obtain converged ground-state energies for UO_2[11] and UN,[16] but have not specifically considered whether U-ramping eliminates metastable states. Additionally, for UN, Claisse *et al.* have shown that convergence to metastable states affects the predicted lattice constants.[16]

Density functionals commonly used for solid-state applications also fail to model the non-local, long-range electron correlations required to accurately model London dispersion interactions.[32–34] While asymptotic dispersion corrections[35–37] provide an accurate and efficient solution to this problem, such corrections are typically not applied to actinide and lanthanide systems. This is most likely because their lattice energies[38,39] are greater than the dispersion energies seen, for example, in layered materials.[40] However, the large atomic size of the actinides should result in large C_6 dispersion coefficients, and previous work has shown that dispersion interactions can significantly affect the volume of ionic solids, such as the alkali halides.[41] Few publications have studied the effect of including a dispersion correction on predicted properties of gas-phase actinide complexes[42–44] and none, to the authors' knowledge, have considered solid-state actinide compounds.

This study investigates the impact of metastable states and dispersion corrections on GGA+U calculations for both structure and thermodynamic properties of four representative uranium compounds (UC, UN, UO_2, and UCl_3). The results show that the range of computed structural properties due to metastable states is typically smaller than variations arising from either the choice of Hubbard U or inclusion of dispersion. Adding a dispersion correction improves the accuracy of the unit-cell geometry and formation enthalpies, such that calculations utilizing high U values best agree with experimental observations. This occurs because the added attractive forces from the dispersion correction balance the repulsive nature of the Hubbard-U correction. In light of these results, a dispersion correction should be included when carrying out GGA+U calculations on actinide and lanthanide compounds.

2 Computational Methods

Spin-polarized DFT calculations were carried out for UC, UN, UO_2, and UCl_3[45] using the projector augmented-wave (PAW) method,[46] as implemented in Quantum ESPRESSO version 6.3.[47] All calculations employed the PBE[48] exchange-correlation functional, with planewave kinetic-energy cut-offs of 130 and 800 Ry for the wavefunctions and electron densities, respectively, and a cold smearing[49] parameter of 0.01 Ry. The PAW datasets used in this paper were taken from PSLibrary version 1.00.[50] While a new set of pseudopotentials has recently been developed specifically for UC,

Figure 1: Crystal unit cells of the four binary uranium compounds studied in this work. Blue: uranium; black: carbon; purple: nitrogen; red: oxygen; green: chlorine. For the two anti-ferromagnetic systems, UN and UO_2, the alternating blue and grey coloring is used for uranium to indicate differing spins.

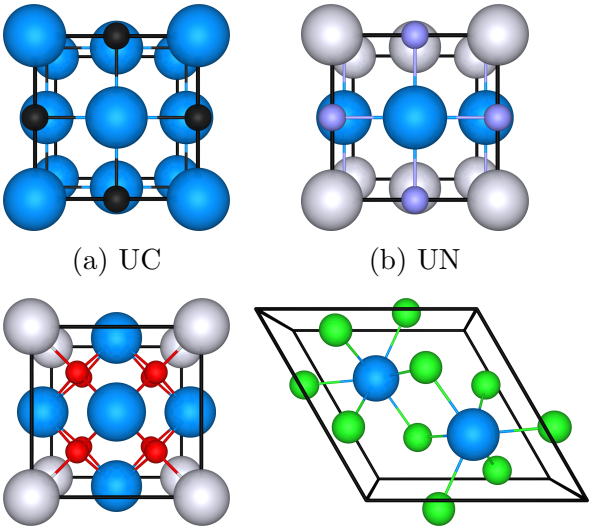

(a) UC (b) UN

(c) UO_2 (d) UCl_3

UN, and UO_2,[51] we continue to use the standard pseudopotentials to maintain consistency with previous computational studies.[9,11–13,52–54] For structural relaxation, a 6×6×6 **k**-point mesh was used for UC, UN, and UO_2, while a 4×4×4 mesh was used for UCl_3. These meshes were found to yield converged calculated structures. Single-point energy calculations required a larger 12×12×12 **k**-point mesh to converge the calculated total energy to within 10^{-6} Ry.

The exchange-hole dipole moment (XDM) model[37,55] was used to evaluate the impact of dispersion interactions on the structures and energetics of these materials. It is added as a correction to the self-consistent energy obtained from the base density functional, in this case PBE:

$$E_{\mathrm{DFT}} = E_{\mathrm{PBE}} + E_{\mathrm{XDM}}. \tag{1}$$

XDM is an asymptotic dispersion correction based on second-order perturbation theory that treats dispersion as arising between instantaneous multipole moments in the electron density of each atom within the system.

The XDM dispersion energy is expressed as a sum over all atom pairs, i and j:

$$E_{\mathrm{XDM}} = -\frac{1}{2}\sum_{\mathbf{L}}\sum_{ij}\sum_{n=6,8,10}\frac{C_{n,ij}f_n^{\mathrm{BJ}}\left(R_{ij,\mathbf{L}}\right)}{R_{ij,\mathbf{L}}^n}, \tag{2}$$

where **L** indicates the lattice vector in a periodic solid and the $i = j$ term is excluded from the sum for $\mathbf{L} = 0$. The Becke-Johnson damping function,[36,56] f_n^{BJ}, prevents divergence of the dispersion correction at small interatomic distances, R_{ij}. It involves only two global parameters, the values of which are dependent on the choice of base functional. Here, these parameters were set to their standard values for use with PBE:[37] $a_1 = 0.3275$ and $a_2 = 2.7673$ Å.

The $C_{n,ij}$ in Eqn. 2 are the dispersion coefficients, which are determined non-empirically from the electron density (ρ) and its derivatives ($\nabla\rho$, $\nabla^2\rho$), as well as the kinetic-energy density (τ). The leading-order C_6 dispersion term accounts for interactions between instantaneous dipole moments. Inclusion of the C_8 and C_{10} terms, arising from interaction of higher-order multipoles, is needed to attain high accuracy for both molecular and solid-state benchmarks.[56–58]

XDM has been shown to provide highly accurate energetics for adsorption of small molecules,[59] and of graphene,[60,61] on transition-metal surfaces, as well as for the interlayer interactions in transition-metal dichalcogenides.[62] Its excellent performance for use with transition metals can be traced to the use of density-dependent dispersion coefficients that include treatment of electronic many-body effects[57] and show large changes in value depending on the atomic chemical environment.[59,62] Given this, XDM is expected to perform well for actinide and lanthanide materials without any modification.

Two sets of structure optimizations involving the Hubbard U correction[27] were performed for each compound: "standard" U-ramping, using default f-orbital occupations, and "variable" U-ramping, where the initial f-orbital occupations were specified and chosen to span all possible combinations. Both sets of calculations were U-ramped in 0.25 eV increments from 0–5 eV, or until the calculations would no longer

converge. The variable-occupancy calculations were carried out for the $\binom{7}{2} = 21$ different combinations of initial f-orbital occupations for the two U^{4+} compounds, UC and UO_2, and for the $\binom{7}{3} = 35$ f-orbital combinations for the U^{3+} compounds, UN and UCl_3. The lowest-energy structure from these relaxations was then used as the input geometry for successive U values.

Both UN and UO_2 were modeled with anti-ferromagnetic ordering, as shown in Figure 1. A transverse $1\mathbf{k}$ anti-ferromagnetic spin arrangement was used for UO_2, as this was found by Pegg et al. to be the preferred magnetic structure.[63] Calculations for UN used a first-order $1\mathbf{k}$ anti-ferromagnetic order, where the uranium atoms change spin for successive layers along the z axis.[64] UCl_3 was treated using ferromagnetic ordering.[65] Calculations for UC converged to paramagnetic solutions at low values of U and to ferromagnetic solutions at high values of U. While an anti-ferromagnetic state has recently been proposed for UC,[66] the precise ordering has not been established and we use the ferromagnetic ordering for consistency with previous computational studies.[17]

Heats of formation were computed using reference free-atom formation enthalpies for the C, N, O, Cl, and U atoms,[67] and DFT atomization enthalpies for the uranium compounds. Single-point energies of the spin-polarized atoms were evaluated using large supercells. For the U atom, calculations were run at each U value for all possible initial combinations of f-orbital occupancies, from which the lowest energy at each U was selected.

For simplicity, thermal enthalpy corrections were calculated within the Debye approximation[68–70] using the Gibbs2 program.[71,72] This model assumes that the phonon density of states is parabolic and its curvature is determined from only the static lattice parameter and bulk modulus. Thus, only the total energy as a function of cell volume is needed to approximate the thermal properties. The Debye model has been used to successfully model thermal contributions to the cell volumes and bulk moduli of alkali halides.[41] Tests were conducted where the thermal enthalpy corrections for the bulk solids were evaluated using PBE and PBE-XDM, with and without a U value of 4.00 eV (or 2.50 eV for UN). However, neither the Hubbard U value nor XDM dispersion corrections were found to affect the thermal enthalpies, so the base PBE values were used in this analysis. The thermal enthalpy correction for the free atoms was taken as $\frac{5}{2}RT$, which is the value for a monoatomic ideal gas. The resulting thermal enthalpy corrections for a temperature of 298.15 K were added to the calculated atomization energies to obtain the standard atomization enthalpies. However, these thermal enthalpy corrections are almost negligible, having values of -0.09 eV for UC and UN, -0.15 eV for UO_2, and -0.18 eV for UCl_3, and could thus be safely neglected in future high-throughput computational studies of actinide thermochemistry.

3 Results and Discussion

3.1 Total Energies and Magnetizations

Total energies of the uranium compounds as a function of Hubbard U are shown in Figure 2. In all cases, the energies increase smoothly with U value, as the additional potential introduces an energy barrier to localize the f-electrons of the uranium. Many metastable states were obtained from the variable-occupancy calculations at high U values, which can lie above the ground state by up to 1 eV per formula unit; the largest range is seen for UO_2. While the standard U-ramping and minimum-energy variable-occupancy results are generally in good agreement, the standard U-ramping calculations failed to converge at high U values for UN, indicating that the variable-occupancy method is more robust, but more computationally expensive.

The focus of metastable states in actinide materials has largely been on UN[8,16,73] and uranium oxides.[9,11–13,52–54] For UO_2 and a U value of 4.5 eV, we identify 9 metastable states with energies of 0.01-0.90 eV (per formula unit) above the ground state. This is in good quantitative agreement with the previous work of Dorado *et al.*,[12] who identified 8 metastable

Figure 2: Relative energies, per formula unit, as a function of U-value for PBE+U and PBE+U-XDM relaxed structures, using both standard and variable U-ramping.

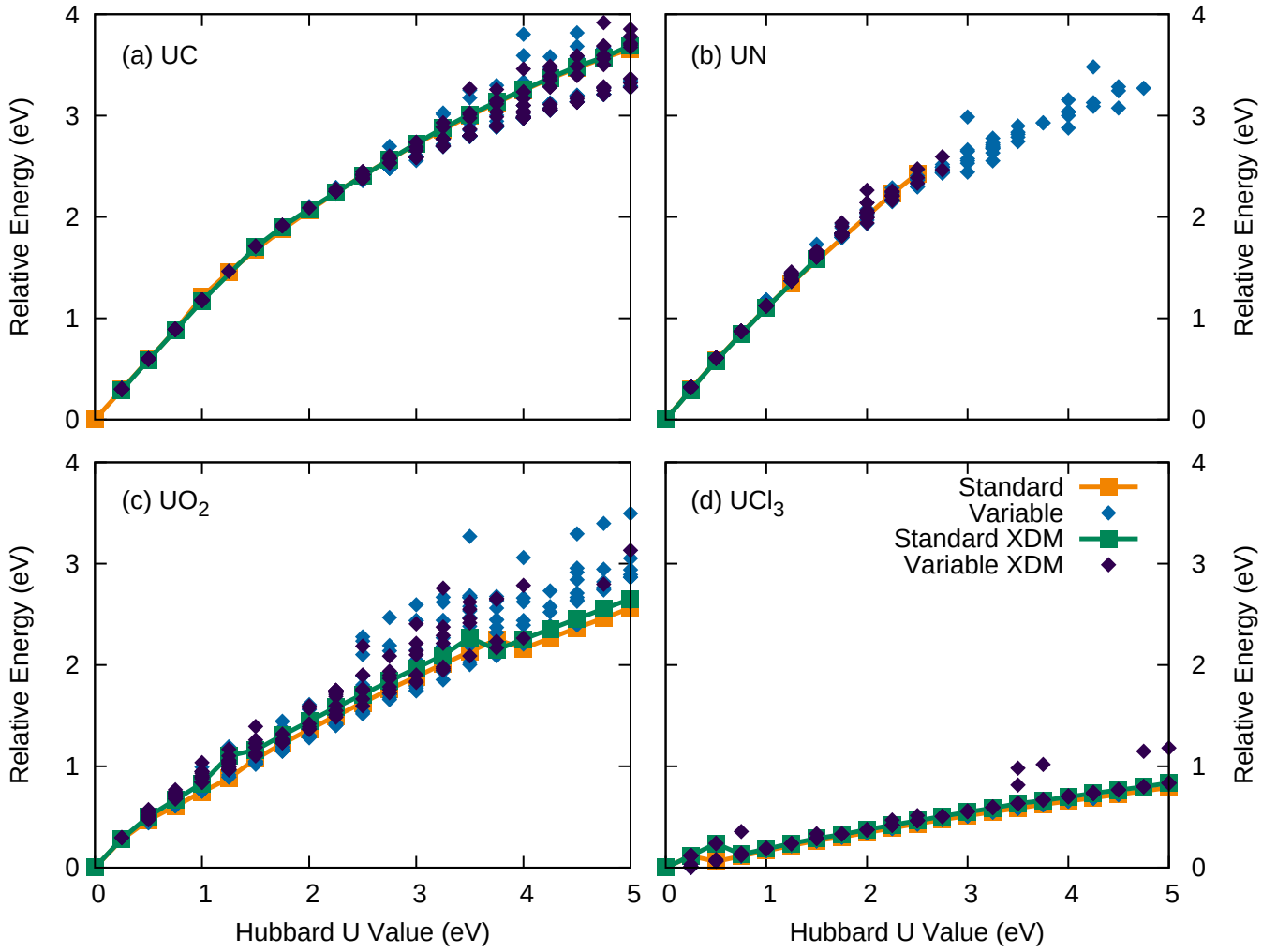

states spanning an energy range of 0.02-0.86 eV above the ground state for the same U value. Similarly, the energy range spanned for the UN metastable states is on par with those reported by Dorado and Claisse.[12,16] We found significantly fewer metastable states for UCl_3 than were seen by Miskowiec for UF_4.[74] Though they are different species, one would expect the nature of the uranium-halide bond to be similar. However, Miskowiec used a fairly low planewave cut-off parameter, while use of sufficiently large cutoffs has been shown to be highly important to minimize generation of metastable states for UO_2.[12] Differences in the number and energy span of metastable states may also be due, in part, to the difference in pseudopotentials between VASP[75] and the PSLibrary.[50] Remaining differences among reported results and the current calculations may be due to these being U-ramped in addition to fixing the initial orbital occupancies.

Finally, the similar trends in relative energies with and without XDM (Figure 2) indicate that the dispersion energy has only a weak dependence on U value. As shown in the Supporting Information, the dispersion energies decrease slightly in magnitude as U value increases. This is due to the increased bond lengths and cell volumes at high U (vide infra) that, in turn, reduce the extent of dispersion stabilization. Despite its dependence on the electron density, the XDM dispersion energy does not vary significantly with the initial orbital occupancy (except for a few metastable states of UCl_3), indicating its relative robustness for actinide chemistry.

Figure 3: Computed absolute magnetizations, per uranium atom, as a function of U-value for PBE+U and PBE+U-XDM relaxed structures, using both standard and variable U-ramping.

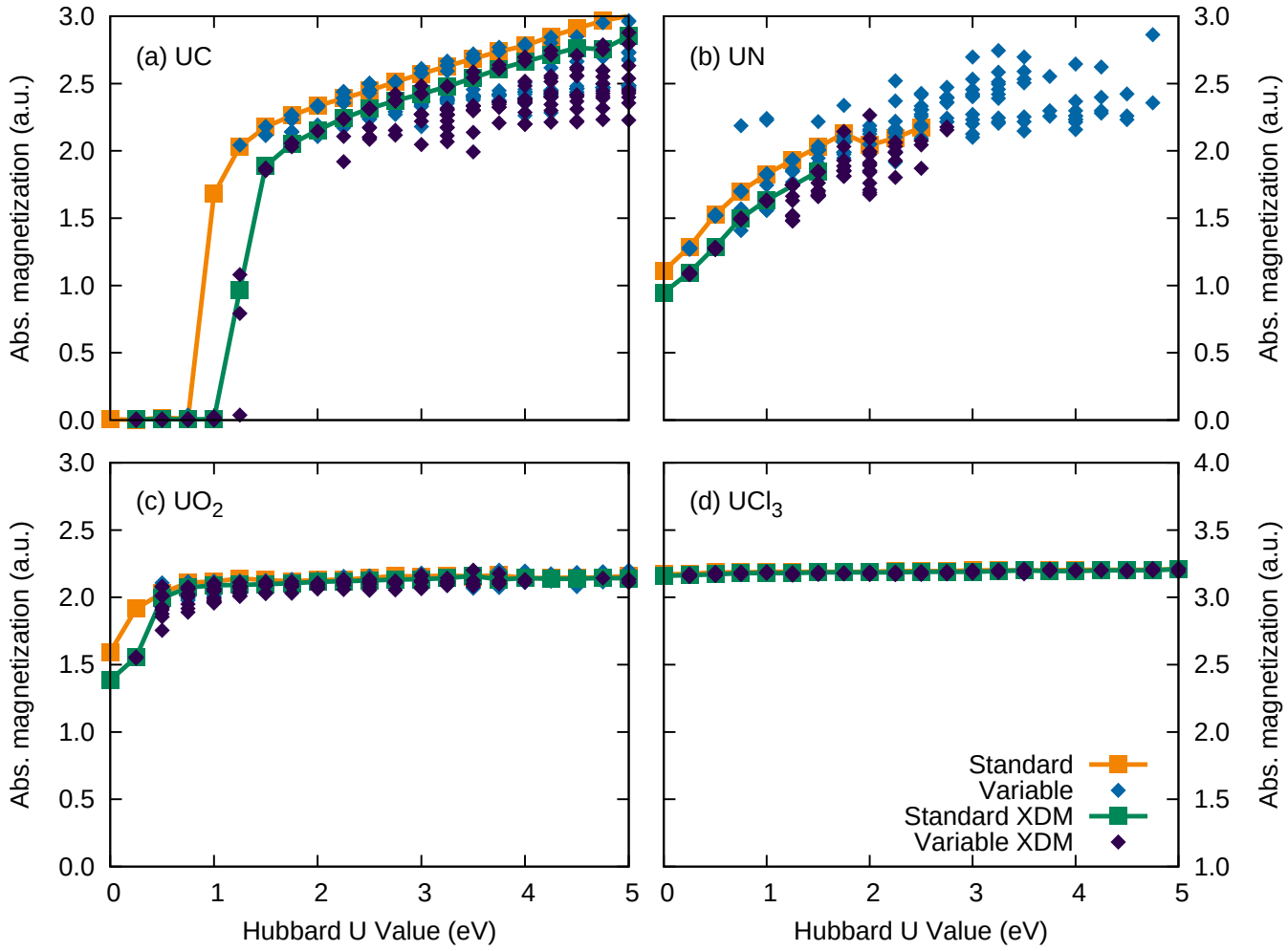

The effect of Hubbard U value on the absolute magnetization for the four uranium compounds is shown in Figure 3. The magnetizations for UO_2 and UCl_3 are largely independent of U value and initial electronic configuration. They approach the idealized values of 2 and 3 expected for U^{4+} and U^{3+} cations, with 2 and 3 unpaired f-shell electrons, respectively. Conversely, the magnetizations of UC and UN, both of which have a rocksalt structure, are strongly dependent on U value and there is also a very large range in the magnetization for the metastable states. Our results shows that UC undergoes a magnetic transition at $U \sim 1$ eV, from a paramagnetic to a ferromagnetic state.

3.2 Cell Geometries

Similar to the total energy, the computed cell volumes were found to increase with U value, as shown in Figure 4. Changes in the individual U–X and U–U bond lengths with U value follow similar trends and are shown in the Supporting Information. The sharp increase in volume seen at $U \sim 1$ eV for UC is a result of the magnetic transition discussed above, and agrees with that reported previously.[17] The larger range of cell volumes for UC and UN is consistent with the existence of many metastable states and the span in cell magnetization seen for these two compounds in Figure 3.

Volume dependence on the metastable-state energy ranking was previously reported by Allen and Watson in their study of CeO_2,[11] and is also seen here. However, the range of cell

Figure 4: Computed cell volumes as a function of U-value for PBE+U and PBE+U-XDM relaxed structures, using both standard and variable U-ramping. The dashed lines represent reference experimental values.[45]

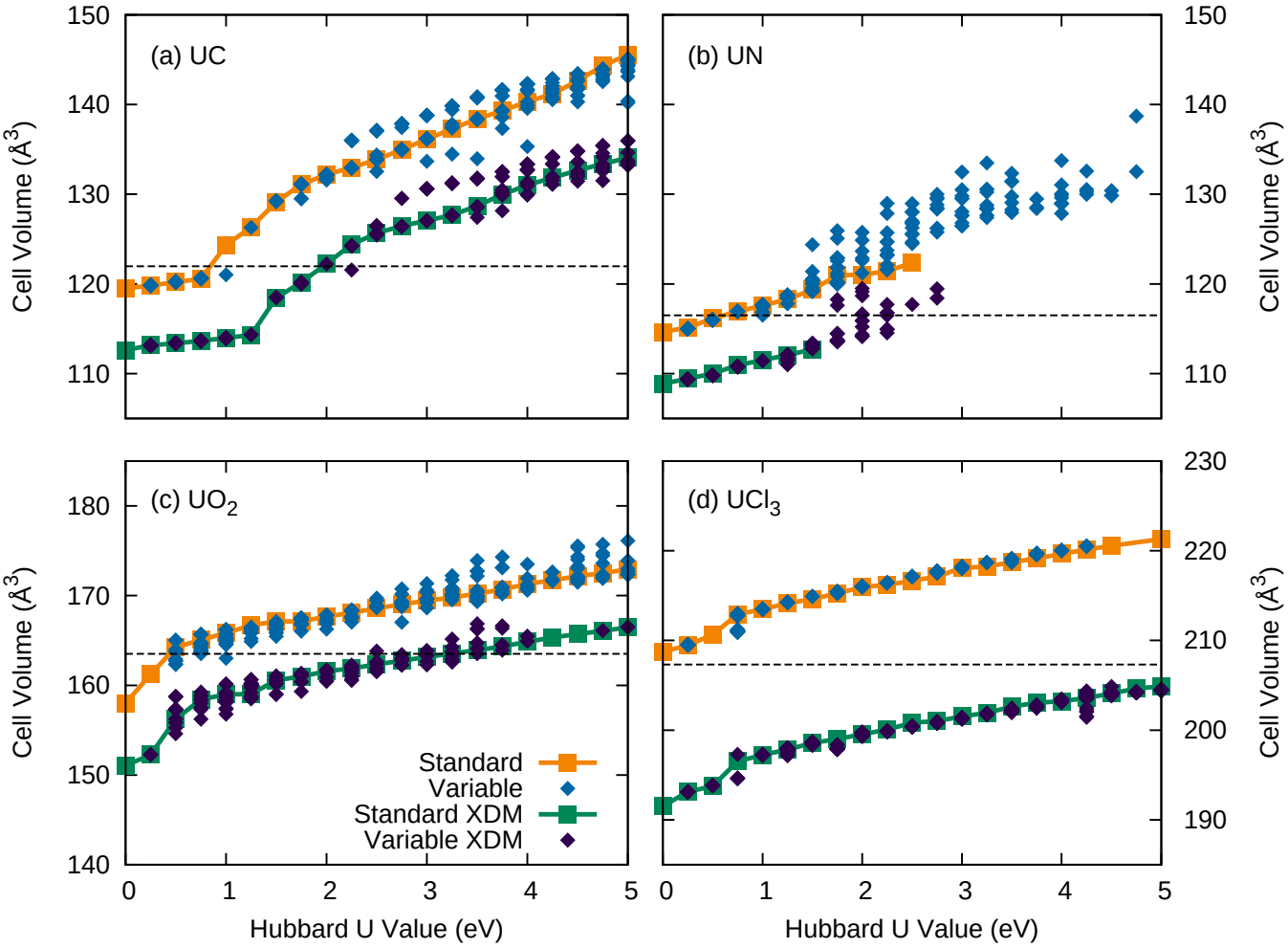

volumes arising from metastable states remain less than the volume changes resulting from increasing U values. Disconnecting structural optimization and energy calculations is important in developing high-throughput methods for f-block materials. The relatively low sensitivity of the cell volumes and bond distances to the electronic configurations means that a composite approach,[76] which couples structural optimization using a low-cost method with high-level PAW single-point energies, could potentially be applied to actinide materials.

The addition of an attractive dispersion interaction naturally results in smaller optimized cell volumes than base-functional-only calculations. Inclusion of XDM dispersion yields shorter U–X (X ∈ C, N, O, Cl) bond lengths by approximately 0.05 Å for each compound. Larger differences, of up to 0.1 Å, are seen for the U-U bond lengths, which is expected since uranium is a much heavier and highly polarizable element and, hence, will be more affected by dispersion. The leading-order C_6 dispersion coefficients range from 700-1000 a.u. for U–U interactions, compared to 50-160 a.u. for U–X interactions, as shown in the Supporting Information.

As noted for the total energies, the effect of dispersion is largely independent of U value. Thus, the PBE+U-XDM curves in Figure 4 have the same shape as those obtained with PBE+U alone, but are uniformly shifted to smaller volumes. For all four compounds considered, the PBE+U results are in good agreement with previous DFT studies,[14,16,17,30] but agree best with experiment only at small U val-

Figure 5: Computed heats of formation, per formula unit, as a function of U-value for PBE+U and PBE+U-XDM relaxed structures, using both standard and variable U-ramping. The dashed lines represent reference experimental values.[77]

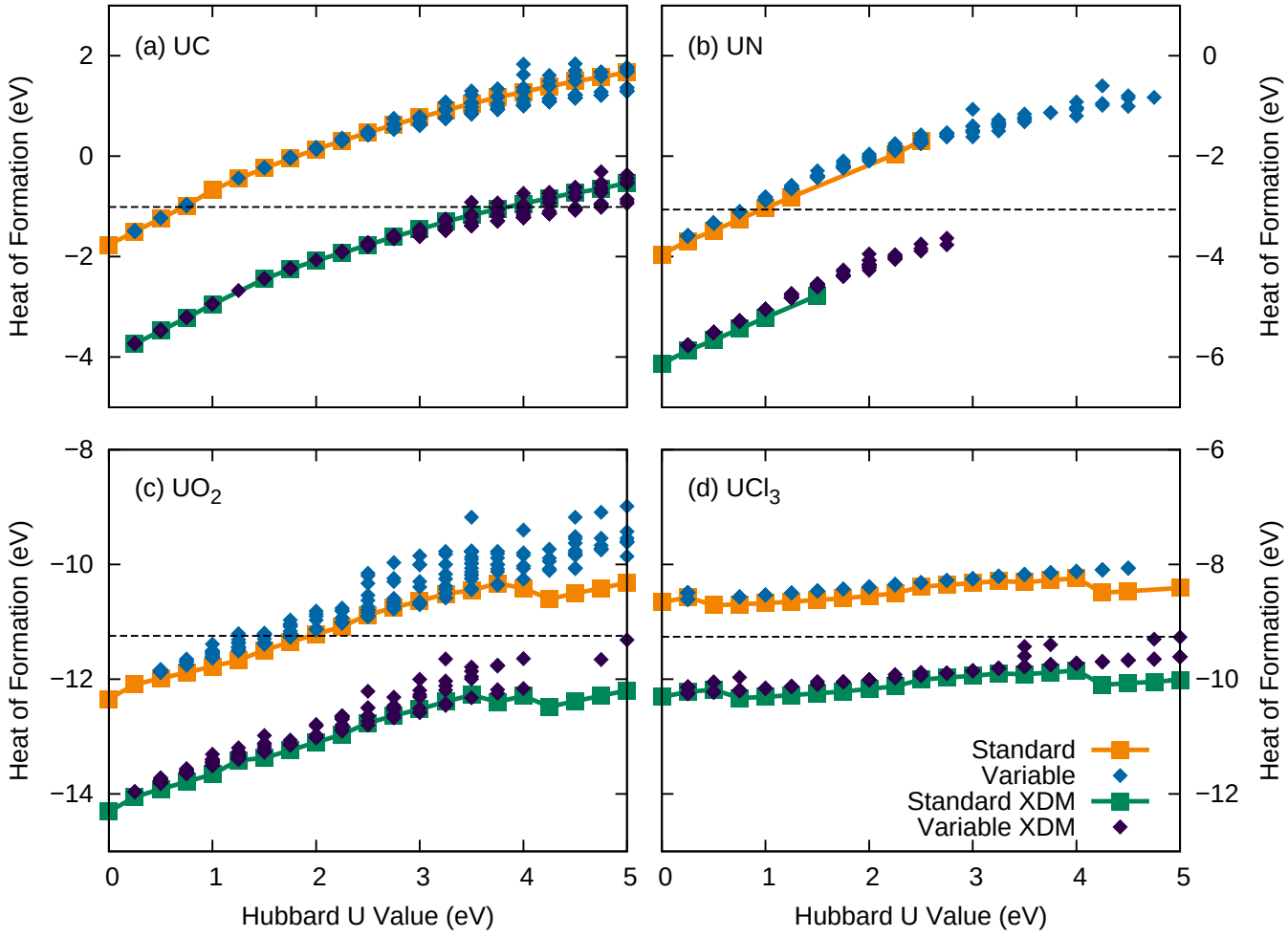

ues. This is in contrast to the typical problem seen in many DFT+U studies, where substantial Hubbard U corrections are required to reproduce experimentally observed properties, such as the band gap. Thus, we have the inconsistent situation of requiring a small or zero U value for accurate prediction of the cell geometry, but a large U value for accurate prediction of the band structure. The attractive dispersion term counterbalances the added repulsion from the Hubbard U corrections, resulting in calculated cell volumes that are closer to experiment when U is above 2 eV. As PBE+U-XDM gives improved agreement with experimental cell volumes and bond lengths at intermediate to high U values, it should simultaneously be capable of providing reasonable geometries and band structures (which are unaffected by the dispersion correction) for a single U value. Additionally, inclusion of thermal expansion effects (neglected here) would expand the computed structures, further decreasing agreement of PBE+U calculations with experiment at high U value, but improving agreement for PBE+U-XDM in the cases of UN and UCl_3.

3.3 Heats of Formation

Computed heats of formation for the four uranium compounds are shown in Figure 5. As for the total energy results, the heats of formation increase with U value, although it should be noted that the U-atom energy is also U dependent. The differences in formation enthalpies between the various metastable states are generally less than the differences resulting from changes in U value. As the forma-

tion enthalpies are computed using atomization energies, and there is no dispersion for an isolated atom, adding the XDM dispersion correction always imparts additional stabilization to the uranium compounds. The XDM correction to the formation enthalpy is approximately 2 eV for each of the four compounds. This energy difference is consistent across the sampled Hubbard-U range, as the XDM energy contribution is effectively U-independent. Thus, the choice of U value and the inclusion of a dispersion correction both play more significant roles in calculating accurate formation enthalpies than does the presence of metastable states.

At small U values of 1-2 eV, PBE+U agrees well with experiment,[77] while PBE+U-XDM strongly overbinds. However, the dispersion correction increases the accuracy of the formation enthalpies at higher U values that are typically used in calculations for these systems.[9,10,28,29,78] The best agreement with the measured formation enthalpies occurs around U = 4 eV, although PBE+U-XDM still slightly overbinds. This behavior is in line with the expected tendency of GGA functionals to overbind, and is consistent with thermochemical benchmarks for small main-group compounds[79,80] and for d-block transition-metal complexes.[81]

To emphase the importance of dispersion for actinide compounds, Figure 6 shows the errors in computed cell volumes and heats of formation obtained with the high U values typically employed for these materials. The Hubbard U correction introduces a repulsion term and PBE+U systematically overestimates the cell volumes by 9.0%. Conversely, the dispersion correction offers additional attractive energy that offsets the repulsive Hubbard U term, providing good agreement with experiment, with a mean error of 1.9% and a mean absolute error of 2.9%. The results would likely be further improved for UN and UCl_3 if thermal expansion were considered. PBE+U also systematically underestimates heats of formation, by 1.33 eV on average. PBE+U-XDM improves agreement with experiment when U is equal to 4.00 eV (2.50 eV for UN), although there

Figure 6: Errors in cell volume and heat of formation of the four binary uranium compounds, using the minimum of the variable-occupancy results with either PBE+U or PBE+U-XDM. The results correspond to typical U values used in literature studies of 4 eV for UC, UO_2, and UCl_3, and 2.5 eV for UN.[2,10,12,82]

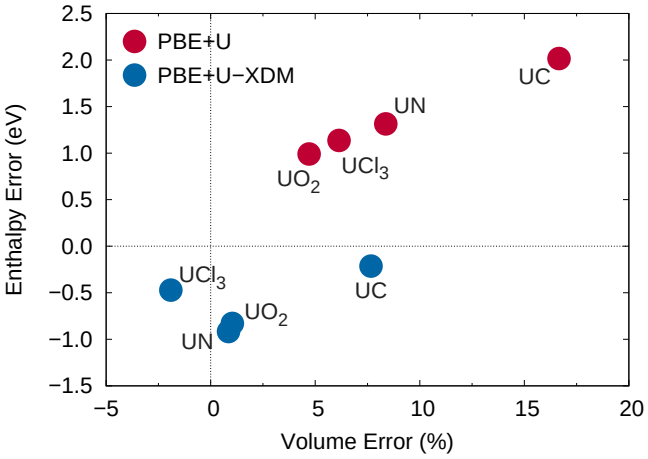

is some residual over-binding expected from a GGA functional, leading to a mean error of −0.64 eV. Therefore, dispersion corrections improve accuracy when using typical actinide U values.

4 Conclusions

A review of the effects of metastable electronic states, choice of Hubbard U values, and the use of the XDM dispersion correction, on structural and thermodynamic properties for UC, UCl_3, UN and UO_2 provides important insights. While possible convergence to metastable states at high U values results in a considerable range of both total energies and absolute magnetization, standard U-ramping is generally able to recover the most stable configuration. However, calculations for UN using standard U-ramping fail to converge at high U values. Physical properties show greater dependence on metastable states for the two rocksalt structures, UC and UN, than for UO_2 and UCl_3. However, the predicted cell volume is generally less sensitive to the presence of metastable states than it is to the effects of both Hubbard U and the addition of a dispersion cor-

rection. This fortuitously suggests that use of approximate methods that concentrate on predicting accurate structures may be useful for high-throughput studies.

Addition of the XDM dispersion correction to standard PBE+U calculations resulted in improved agreement in computed cell volumes and formation enthalpies with experimental values for the four uranium compounds studied. This occurs because the added dispersion attraction counterbalances the repulsive Hubbard U correction. Thus, a dispersion correction is required to obtain accurate structural and thermodynamic properties for actinide compound calculations using typical, high U values required to obtain accurate description of their band structures. Additionally, changes in both the initial orbital occupations and choice of U value were shown to have little effect on the XDM dispersion correction, allowing its effective use with f-block elements.

Acknowledgement E.R.J. thanks the Natural Sciences and Engineering Research Council of Canada (NSERC) for financial support. M.S.C. and T.M.B. thank the U.S. Department of Energy, Office of Science, Basic Energy Sciences, under Award No. DE-SC0016574 (Center for Hierarchical Waste Form Materials), as well as the Nuclear Energy University Program of the US Department of Energy, under Award ID: DE-NE0008772, 18-15065 (In Situ Measurement and Validation of Uranium Molten Salt Properties at Operationally Relevant Temperatures). This research used computational resources provided by the National Energy Research Scientific Computing Center (NERSC) and the HPC cluster Hyperion, supported by the Division of Information Technology at the University of South Carolina.

Supporting Information Available: Table of C_6 dispersion coefficients; plots of the dispersion energy, U-X, and U-U bond lengths as functions of Hubbard U parameter. This material is available free of charge via the Internet at `http://pubs.acs.org/`.

References

(1) Ewing, R. C. Nuclear Waste Forms for Actinides. *Proc. Natl. Acad. Sci. U. S. A.* **1999**, *96*, 3432–3439.

(2) Ji, Y.; Beridze, G.; Li, Y.; Kowalski, P. M. Large Scale Simulation of Nuclear Waste Materials. *Energy Procedia* **2017**, *127*, 416–424.

(3) Bragg-Sitton, S. M.; Todosow, M.; Montgomery, R.; Stanek, C. R.; Montgomery, R.; Carmack, W. J. Metrics for the Technical Performance Evaluation of Light Water Reactor Accident-Tolerant Fuel. *Nuclear Technology* **2016**, 111–123.

(4) Greeley, J.; Nørskov, J. K. Large-Scale, Density Functional Theory-Based Screening of Alloys for Hydrogen Evolution. *Surf. Sci.* **2007**, *601*, 1590–1598.

(5) Lu, J. W.; Chang, N. B.; Liao, L. Environmental Informatics for Solid and Hazardous Waste Management: Advances, Challenges, and Perspectives. *Crit. Rev. Environ. Sci. Technol.* **2013**, *43*, 1557–1656.

(6) Wu, H.; Mayeshiba, T.; Morgan, D. High-Throughput ab-initio Dilute Solute Diffusion Database. *Sci. Data* **2016**, *3*, 1–11.

(7) Kirklin, S.; Saal, J. E.; Hegde, V. I.; Wolverton, C. High-Throughput Computational Search for Strengthening Precipitates in Alloys. *Acta Mater.* **2016**, *102*, 125–135.

(8) Liu, X. Y.; Andersson, D. A.; Uberuaga, B. P. First-Principles DFT Modeling of Nuclear Fuel Materials. *J. Mater. Sci.* **2012**, *47*, 7367–7384.

(9) Dorado, B.; Freyss, M.; Amadon, B.; Bertolus, M.; Jomard, G.; Garcia, P. Advances in First-Principles Modelling of Point Defects in UO_2: F electron Correlations and the Issue of Local Energy Minima. *J. Phys. Condens. Matter* **2013**, *25*, 333201–333214.

(10) Beridze, G.; Kowalski, P. M. Benchmarking the DFT+U Method for Thermochemical Calculations of Uranium Molecular Compounds and Solids. *J. Phys. Chem. A* **2014**, *118*, 11797–11810.

(11) Allen, J. P.; Watson, G. W. Occupation Matrix Control of d- and f-Electron Localisations using DFT+U. *Phys. Chem. Chem. Phys.* **2014**, *16*, 21016–21031.

(12) Dorado, B.; Amadon, B.; Freyss, M.; Bertolus, M. DFT+U Calculations of the Ground State and Metastable States of Uranium Dioxide. *Phys. Rev. B* **2009**, *79*, 1–8.

(13) Devey, A. J. First Principles Calculation of the Elastic Constants and Phonon Modes of UO_2 Using GGA+U with Orbital Occupancy Control. *J. Nucl. Mater.* **2011**, *412*, 301–307.

(14) Gryaznov, D.; Heifets, E.; Kotomin, E. The First-Principles Treatment of the Electron-Correlation and Spin-Orbital Effects in Uranium Mononitride Nuclear Fuels. *Phys. Chem. Chem. Phys.* **2012**, *14*, 4482–4490.

(15) Mei, Z. G.; Stan, M.; Pichler, B. First-Principles Study of Structural, Elastic, Electronic, Vibrational and Thermodynamic Properties of UN. *J. Nucl. Mater.* **2013**, *440*, 63–69.

(16) Claisse, A.; Klipfel, M.; Lindbom, N.; Freyss, M.; Olsson, P. GGA+U Study of Uranium Mononitride: A Comparison of the U-ramping and Occupation Matrix Schemes and Incorporation Energies of Fission Products. *J. Nucl. Mater.* **2016**, *478*, 119–124.

(17) Mankad, V. H.; Jha, P. K. Thermodynamic Properties of Nuclear Material Uranium Carbide Using Density Functional Theory. *J. Therm. Anal. Calorim.* **2016**, *124*, 11–20.

(18) Perdew, J. P. et al. Understanding band gaps of solids in generalized Kohn-Sham theory. *Proc. Natl. Acad. Sci.* **2017**, *114*, 2801–2806.

(19) Ángel Morales-García,; Valero, R.; Illas, F. An Empirical, yet Practical Way To Predict the Band Gap in Solids by Using Density Functional Band Structure Calculations. *J. Phys. Chem. C* **2017**, *121*, 18862–18866.

(20) Tran, F.; Blaha, P. Importance of the Kinetic Energy Density for Band Gap Calculations in Solids with Density Functional Theory. *J. Phys. Chem. A* **2017**, *121*, 3318–3325.

(21) Cohen, A. J.; Mori-Sánchez, P.; Yang, W. Fractional charge perspective on the band gap in density-functional theory. *Phys. Rev. B.* **2008**, *77*, 115123.

(22) Mori-Sánchez, P.; Cohen, A. J.; Yang, W. Localization and Delocalization Errors in Density Functional Theory and Implications for Band-Gap Prediction. *Phys. Rev. Lett.* **2008**, *100*, 146401.

(23) Kim, M.-C.; Sim, E.; Burke, K. Understanding and reducing errors in density functional calculations. *Phys. Rev. Lett.* **2013**, *111*, 073003.

(24) Dudarev, S. L.; Botton, G. A.; Savrasov, S. Y.; Humphreys, C. J.; Sutton, A. P. Electron-energy-loss spectra and the structural stability of nickel oxide:An LSDA+U study. *Phys. Rev. B* **1998**, *57*, 1505–1509.

(25) Kulik, H. J. Treating electron overdelocalization with the DFT+U method. *J. Chem. Phys.* **2015**, *142*, 240901.

(26) Himmetoglu, B.; Floris, A.; de Gironcoli, S.; Cococcioni, M. Hubbardcorrected DFT energy functionals: The LDA+U description of correlated systems. *Int. J. Quantum Chem.* **2014**, *114*, 14–49.

(27) Cococcioni, M.; De Gironcoli, S. Linear Response Approach to the Calculation of the Effective Interaction Parameters in the

LDA+U Method. *Phys. Rev. B* **2005**, *71*, 1–16.

(28) Beridze, G.; Birnie, A.; Koniski, S.; Ji, Y.; Kowalski, P. M. DFT+U as a Reliable Method for Efficient ab initio Calculations of Nuclear Materials. *Prog. Nucl. Energy* **2016**, *92*, 142–146.

(29) Dorado, B.; Andersson, D. A.; Stanek, C. R.; Bertolus, M.; Uberuaga, B. P.; Martin, G.; Freyss, M.; Garcia, P. First-Principles Calculations of Uranium Diffusion in Uranium Dioxide. *Phys. Rev. B* **2012**, *86*, 035110–034124.

(30) Meredig, B.; Thompson, A.; Hansen, H. A.; Wolverton, C.; van de Walle, A. Method for Locating Low-Energy Solutions Within DFT+U. *Phys. Rev. B* **2010**, *82*, 195128–195133.

(31) Geng, H. Y.; Chen, Y.; Kaneta, Y.; Kinoshita, M.; Wu, Q. Interplay of Defect Cluster and the Stability of Xenon in Uranium Dioxide from Density Functional Calculations. *Phys. Rev. B* **2010**, *82*, 1–9.

(32) Klimeš, J.; Michaelides, A. Perspective: Advances and Challenges in Treating van der Waals Dispersion Forces in Density Functional Theory. *J. Chem. Phys.* **2012**, *137*, 120901.

(33) Grimme, S.; Hansen, A.; Brandenburg, J. G.; Bannwarth, C. Dispersion-Corrected Mean-Field Electronic Structure Methods. *Chem. Rev.* **2016**, *116*, 5105–5154.

(34) Hermann, J.; DiStasio Jr., R. A.; Tkatchenko, A. First-Principles Models for van der Waals Interactions in Molecules and Materials: Concepts, Theory, and Applications. *Chem. Rev.* **2017**, *117*, 4714–4758.

(35) Grimme, S.; Antony, J.; Ehrlich, S.; Krieg, H. A consistent and accurate ab initio parametrization of density functional dispersion correction (DFT-D) for the 94 elements H-Pu. *J. Chem. Phys.* **2010**, *132*, 154104.

(36) Grimme, S.; Ehrlich, S.; Goerigk, L. Effect of the damping function in dispersion corrected density functional theory. *J. Comput. Chem.* **2011**, *32*, 1456–1465.

(37) Johnson, E. R. In *Non-covalent Interactions in Quantum Chemistry and Physics*; Otero-de-la-Roza, A., DiLabio, G. A., Eds.; Elsevier, 2017; Chapter 5, pp 169–194.

(38) Lide, D., Haynes, W., Eds. *CRC handbook of chemistry and physics, 90th edition*; CRC Press, 2010.

(39) Catlow, C. R. A. Theoretical Studies of Cohesive, Electronic and Redox Properties of Uranium Dioxide. *J. Chem. Soc. Faraday Trans. 2* **1978**, *74*, 1901–1908.

(40) Björkman, T. Testing several recent van der Waals density functionals for layered structures. *J. Chem. Phys.* **2014**, *141*, 074708.

(41) Otero-de-la Roza, A.; Johnson, E. R. Application of XDM to ionic solids: the importance of dispersion for bulk moduli and crystal geometries. *J. Chem. Phys.* **2020**, *153*, 054121.

(42) Reta, D.; Ortu, F.; Randall, S.; Mills, D. P.; Chilton, N. F.; Winpenny, R. E.; Natrajan, L.; Edwards, B.; Kaltsoyannis, N. The Performance of Density Functional Theory for the Description of Ground and Excited State Properties of Inorganic and Organometallic Uranium Compounds. *J. Organomet. Chem.* **2018**, *857*, 58–74.

(43) Pandey, K. K. The Effect of Density Functional and Dispersion Interaction on Structure and Bonding Analysis of Uranium(VI) Nitride Complex [N≡U{N($CH_2CH_2NSiMe_3$)$_3$}]: A Theoretical Study. *Inorg. Chem. Commun.* **2013**, *37*, 4–6.

(44) Pandey, K. K.; Patidar, P.; Patidar, S. K.; Vishwakarma, R. Effects of Density Functionals and Dispersion Interactions on Geometries, Bond Energies and Harmonic Frequencies of EUX_3 (E = N, P, CH; X = H, F, Cl). *Spectrochim. Acta - Part A* **2014**, *133*, 846–855.

(45) Zachariasen, W. H. The UCl_3 Type of Crystal Structure. *J. Chem. Phys.* **1948**, *16*, 254–254.

(46) Blöchl, P. E. Projector augmented-wave method. *Phys. Rev. B* **1994**, *50*, 17953.

(47) Giannozzi, P. et al. Advanced capabilities for materials modelling with Quantum ESPRESSO. *J. Phys.: Condens. Matter* **2017**, *29*, 465901.

(48) Perdew, J.; Burke, K.; Ernzerhof, M. Generalized gradient approximation made simple. *Phys. Rev. Lett.* **1996**, *77*, 3865–3868.

(49) Marzari, N.; Vanderbilt, D.; De Vita, A.; Payne, M. C. Thermal Contraction and Disordering of the Al(110) Surface. *PRL* **1999**, *82*, 3296–3299.

(50) Dal Corso, A. Pseudopotentials periodic table: From H to Pu. *Comp. Mat. Sci.* **2014**, *95*, 337–350.

(51) Torres, E.; Kaloni, T. Projector augmented-wave pseudopotentials for uranium-based compounds. *Comp. Mat. Sci.* **2020**, *171*, 109237.

(52) Rabone, J.; Krack, M. A Procedure for Bypassing Metastable States in Local Basis Set DFT+U Calculations and its Application to Uranium Dioxide Surfaces. *Comput. Mater. Sci.* **2013**, *71*, 157–164.

(53) Talla Noutack, M. S.; Geneste, G.; Jomard, G.; Freyss, M. First-Principles Investigation of the Bulk Properties of Americium Dioxide and Sesquioxides. *Phys. Rev. Mater.* **2019**, *3*, 1–13.

(54) Torres, E.; Kaloni, T. P. Thermal Conductivity and Diffusion Mechanisms of Noble Gases in Uranium Dioxide: A DFT+U study. *J. Nucl. Mater.* **2019**, *521*, 137–145.

(55) Otero-de-la-Roza, A.; Johnson, E. R. Van der Waals interactions in solids using the exchange-hole dipole moment. *J. Chem. Phys.* **2012**, *136*, 174109.

(56) Johnson, E. R.; Becke, A. D. A post-Hartree-Fock model of intermolecular interactions: Inclusion of higher-order corrections. *J. Chem. Phys.* **2006**, *124*, 174104.

(57) Otero-de-la Roza, A.; LeBlanc, L. M.; Johnson, E. R. What Is Many-Body Dispersion and Should I Worry About It? *Phys. Chem. Chem. Phys.* **2020**, *22*, 8266–8276.

(58) Otero-de-la-Roza, A.; Johnson, E. R. Predicting energetics of supramolecular systems using the XDM dispersion model. *J. Chem. Theory Comput.* **2015**, *11*, 4033–4040.

(59) Christian, M. S.; Otero-de-la-Roza, A.; Johnson, E. R. Surface adsorption from the exchange-hole dipole moment dispersion model. *J. Chem. Theory Comput.* **2016**, *12*, 3305.

(60) Christian, M. S.; Otero-de-la-Roza, A.; Johnson, E. R. Adsorption of graphene to nickel (111) using the exchange-hole dipole moment model. *Carbon* **2017**, *118*, 184–191.

(61) Christian, M. S.; Otero-de-la-Roza, A.; Johnson, E. R. Adsorption of graphene to metal (111) surfaces using the exchange-hole dipole moment model. *Carbon* **2017**, *124*, 531–540.

(62) Otero-de-la-Roza, A.; LeBlanc, L. M.; Johnson, E. R. Pairwise Dispersion Corrections Can Describe Layered Materials Accurately. *J. Phys. Chem. Lett.* **2020**, *11*, 2298–2302.

(63) Pegg, J. T.; Aparicio-Anglès, X.; Storr, M.; de Leeuw, N. H. DFT+U Study of the Structures and Properties of the Actinide Dioxides. *J. Nucl. Mater.* **2017**, *492*, 269–278.

(64) Curry, N. A. An Investigation of the Magnetic Structure of Uranium Nitride by Neutron Diffraction. *Proc. Phys. Soc.* **1965**, *86*, 1193–1198.

(65) Kindra, D. R.; Evans, W. J. Magnetic Susceptibility of Uranium Complexes. *Chem. Rev.* **2014**, *114*, 8865–8882.

(66) Wdowik, U. D.; Piekarz, P.; Legut, D.; Jagło, G. Effect of Spin-Orbit and On-Site Coulomb Interactions on the Electronic Structure and Lattice Dynamics of Uranium Monocarbide. *Phys. Rev. B* **2016**, *94*, 1–9.

(67) Linstrom, P. J., Mallard, W. G., Eds. *NIST chemistry webbook, NIST Standard Reference Database Number 69*; National Institute of Standards and Technology Washington, Gaithersburg MD, 20899, 2019.

(68) Debye, P. Concerning the theory of specific heat. *Ann. Physik* **1912**, *39*, 789–839.

(69) Ashcroft, N. W.; Mermin, N. D. *Solid state physics*; Thomson Learning Inc., 1976.

(70) Blanco, M.; Francisco, E.; Luana, V. GIBBS: isothermal-isobaric thermodynamics of solids from energy curves using a quasi-harmonic Debye model. *Comput. Phys. Commun.* **2004**, *158*, 57–72.

(71) Otero-de-la Roza, A.; Luaña, V. Gibbs2: A new version of the quasi-harmonic model code. I. Robust treatment of the static data. *Comput. Phys. Commun.* **2011**, *182*, 1708–1720.

(72) Otero-de-la-Roza, A.; Abbasi-Pérez, D.; Luaña, V. Gibbs2: A new version of the quasiharmonic model code. II. Models for solid-state thermodynamics, features, and implementation. *Comp. Phys. Comm.* **2011**, *182*, 2232–2248.

(73) Schuler, T.; Lopes, D. A.; Claisse, A.; Olsson, P. Transport Properties of C and O in UN Fuels. *Phys. Rev. B* **2017**, *95*, 094117–094130.

(74) Miskowiec, A. Metastable Electronic States in Uranium Tetrafluoride. *Phys. Chem. Chem. Phys.* **2018**, *20*, 10384–10395.

(75) Kresse, G.; Furthmüller, J. Efficient Iterative Schemes for ab initio Total-Energy Calculations Using a Plane-Wave Basis Set. *Phys. Rev. B* **1996**, *54*, 11169.

(76) LeBlanc, L. M.; Otero-de-la-Roza, A.; Johnson, E. R. Composite and Low-Cost Approaches for Molecular Crystal Structure Prediction. *J. Chem. Theory Comput.* **2018**, *14*, 2265–2276.

(77) Grenthe, I.; Fuger, J.; Lemire, R. J.; Muller, A. B.; Wanner, H.; Forest, I. *Chemical Thermodynamics of Uranium*; Nuclear Energy Agency Organisation for Economic Co-Operation and Development, 1992.

(78) Kaur, G.; Panigrahi, P.; Valsakumar, M. C. Thermal Properties of UO_2 with a Non-Local Exchange-Correlation Pressure Correction: A Systematic First Principles DFT+U study. *Model. Simul. Mater. Sci. Eng.* **2013**, *21*, 065014–065028.

(79) Curtiss, L. A.; Raghavachari, K.; Redfern, P. C.; Pople, J. A. Assessment of Gaussian-2 and density functional theories for the computation of enthalpies of formation. *J. Chem. Phys.* **1997**, *106*, 1063–1079.

(80) Becke, A. D. Density-functional thermochemistry. III. The role of exact exchange. *J. Chem. Phys.* **1993**, *98*, 5648–5652.

(81) Otero-de-la-Roza, A.; Johnson, E. R. Non-Covalent Interactions and Thermochemistry using XDM-Corrected Hybrid and

Range-Separated Hybrid Density Functionals. *J. Chem. Phys.* **2013**, *138*, 204109.

(82) Dorado, B.; Garcia, P. First-Principles DFT+U Modeling of Actinide-Based Alloys: Application to Paramagnetic Phases of UO_2 and (U,Pu) Mixed Oxides. *Phys. Rev. B* **2013**, *87*, 18–20.

Graphical TOC Entry